Meteoritics & Planetary Science 41, Nr 7, 1027–1038 (2006)
Abstract available online at http://meteoritics.org

A relict-grain-bearing porphyritic olivine compound chondrule from LL3.0 Semarkona that experienced limited remelting

Alan E. RUBIN

Institute of Geophysics and Planetary Physics, University of California–Los Angeles, Los Angeles, California 90095–1567, USA
E-mail: aerubin@ucla.edu

(Received 09 February 2006; revision accepted 24 April 2006)

Abstract–Chondrule D8n in LL3.0 Semarkona is a porphyritic olivine (PO) chondrule, 1300 × 1900 µm in size, with a complicated thermal history. The oldest recognizable portion of D8n is a moderately high-FeO, PO chondrule that is modeled as having become enmeshed in a dust ball containing a small, intact, low-FeO porphyritic chondrule and fine-grained material consisting of forsterite, kamacite, troilite, and possibly reduced C. The final chondrule melting event may have been a heat pulse that preferentially melted the low-FeO material and produced a low-FeO, opaque-rich, exterior region, 45–140 µm in thickness, around the original chondrule. At one end of the exterior region, a kamacite- and troilite-rich lump 960 µm in length formed. During the final melting event, the coarse, moderately ferroan olivine phenocrysts within the original chondrule appear to have been partly resorbed (These relict phenocrysts have the highest concentrations of FeO, MnO, and Cr_2O_3—7.5, 0.20, and 0.61 wt%, respectively—in D8n.). Narrow olivine overgrowths crystallized around the phenocrysts following final chondrule melting; their compositions seem to reflect mixing between melt derived from the exterior region and the resorbed margins of the phenocrysts. During the melting event, FeO in the relict phenocrysts was reduced, producing numerous small blebs of Ni-poor metallic Fe along preexisting curvilinear fractures. The reduced olivine flanking the trails of metal blebs has lower FeO than the phenocrysts but virtually identical MnO and Cr_2O_3 contents. Subsequent parent-body aqueous alteration in the exterior region of the chondrule formed pentlandite and abundant magnetite.

INTRODUCTION

Some researchers have modeled porphyritic chondrules with euhedral phenocrysts as having formed from droplets that experienced high degrees of melting during a single heating episode (e.g., Lofgren and Russell 1986; Hewins 1988; Lofgren 1989; Yu and Hewins 1998). This model can be tested by studies of relict grains inside chondrules, i.e., those grains that survived the final chondrule melting event. Many porphyritic chondrules contain relict grains (e.g., Nagahara 1981; Rambaldi 1981; Rambaldi and Wasson 1982; Kracher et al. 1984; Jones 1996; Wasson and Rubin 2003) that served as nucleation sites for overgrowths of mafic phases that crystallized from the final chondrule melt.

The two most common varieties of relict grains are 1) low-FeO relicts with high-FeO overgrowths inside high-FeO porphyritic chondrules, and 2) high-FeO "dusty" olivine phenocrysts with low-FeO overgrowths inside low-FeO porphyritic chondrules:

1. Nearly every high-FeO porphyritic chondrule in CO3 chondrites (and many in type 3 ordinary chondrites) contains low-FeO relict olivine grains surrounded by narrow overgrowths of ferroan olivine, ~5 µm in thickness (Steele 1989; Jones 1990, 1992; Wasson and Rubin 2003). The overgrowths are similar in their fayalitic compositions and in their O-isotopic compositions to the outer zones of ferroan olivine phenocrysts in the host chondrule (Kunihiro et al. 2004). The low-FeO relict grains are generally similar in their chemical and O-isotopic composition to low-FeO porphyritic chondrules (Jones et al. 2000; Kunihiro et al. 2004).
2. High-FeO "dusty" olivine phenocrysts with low-FeO overgrowths that occur in low-FeO chondrules constitute ~10% of ordinary-chondrite (OC) chondrules (Nagahara 1983; Grossman et al. 1988). The high-FeO relict grains appear dusty when viewed in transmitted light; they commonly consist of numerous micrometer-sized, low-

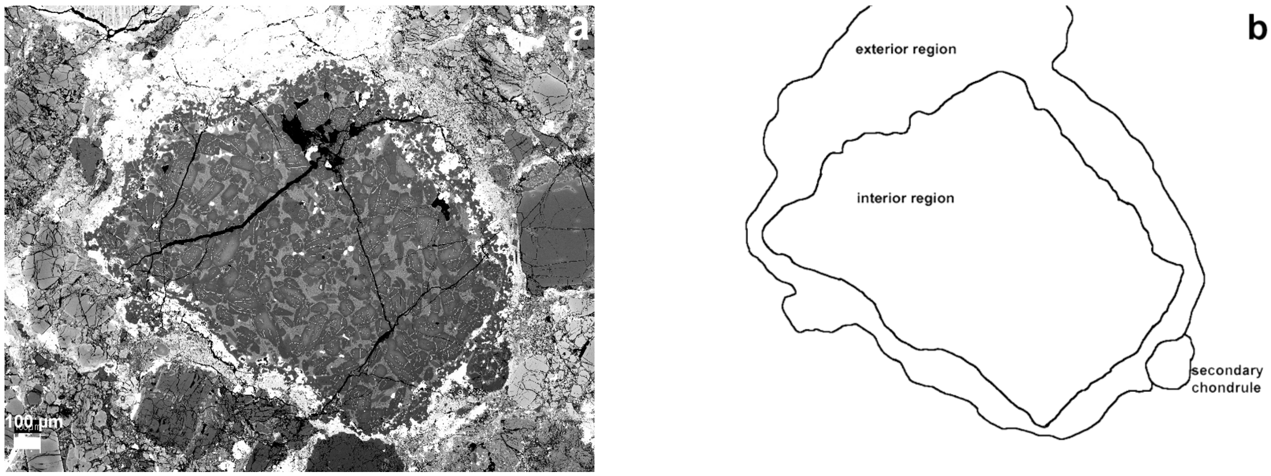

Fig. 1. The porphyritic chondrule D8n. a) A backscattered electron (BSE) image. The interior region of the chondrule contains numerous olivine phenocrysts replete with curvilinear trails of metallic Fe blebs. The exterior region of the chondrule contains olivine grains and abundant clusters of metal and sulfide. Attached to this region at bottom right is a small, round, secondary chondrule. At the upper left is a large opaque nodule (white) at the chondrule margin that is not easily distinguished in this image. b) A schematic diagram of chondrule D8n showing the boundaries of the different regions.

Ni metallic Fe blebs within moderately FeO-rich olivine grains inside low-FeO porphyritic chondrules (Nagahara 1981; Rambaldi 1981; Rambaldi and Wasson 1982). The metal blebs typically constitute 2–8 vol% of the relict olivine grains (Jones and Danielson 1995). Most dusty olivine cores are rimmed by metal-free olivine overgrowths, 4–8 µm in thickness, similar in composition to non-dusty olivine phenocrysts in the host chondrule.

In the present study, I describe an unusual high-FeO porphyritic olivine chondrule with high-FeO dusty relict grains with low-FeO overgrowths in the LL3.0 chondrite Semarkona. The chondrule contains metal blebs (formed by reduction) that occur in widely separated curvilinear arrays, making analysis of adjacent olivine feasible and allowing the extent of reduction to be determined precisely. The inferred petrogenetic history of the chondrule offers broad constraints on chondrule cooling rates and provides information on the stochastic nature of the compositional evolution of solids in the solar nebula.

ANALYTICAL PROCEDURES

I examined thin section AMNH 4128-2 of LL3.0 Semarkona in transmitted light and in backscattered electron (BSE) images. I used a mosaic image of the thin section with a superposed location grid to label chondrules. BSE images were made with the LEO 1430VP scanning electron microscope (SEM) at UCLA using a 15 keV acceleration voltage and a working distance of ~19 mm. Chondrule and grain sizes were measured on the BSE images using the automated scale. Silicate and metallic phase compositions were determined with the JEOL JXA-8200 electron microprobe at UCLA using natural and synthetic standards, an accelerating voltage of 15 keV, a 15 nA sample current, 20 s counting times per element, and ZAF corrections. Minerals were analyzed with a focused beam; mesostasis was analyzed with a beam 5 µm in diameter. Analyses with totals outside the range 98.5–101.5 wt% were discarded. Metal analyses with 0.10 wt% Si, signifying significant overlap of the electron beam on adjacent silicate grains, were also discarded. A single analysis was made of each grain.

RESULTS

Petrography and Mineralogy of Chondrule D8n

Chondrule D8n is a 1300 × 1900 µm porphyritic olivine (PO) chondrule (Fig. 1a) that is divided into a silicate-rich interior region and an opaque-rich exterior region (Fig. 1b). A circular object 170 µm in diameter (which seems to be a secondary chondrule) occurs at the outer margin of the exterior region. If I assume arbitrarily that the radius of the third dimension outside the plane of the section is equal to the mean of the two dimensions within the section, the chondrule can be modeled as a tri-axial ellipsoid. In that case, the exterior and interior regions would each constitute ~50 vol% of the entire chondrule.

Interior Region

The interior consists of ~55 vol% olivine, ~10 vol% low-Ca pyroxene, ~2 vol% Ca-rich pyroxene (occurring as rims on the low-Ca pyroxene grains), ~3 vol% metallic Fe-Ni and troilite (present mainly as blebs in the mesostasis), and ~30 vol% mesostasis. Silicate compositions are listed in Table 1.

Some olivine phenocrysts in the interior are euhedral; others are subhedral. They range in size from 30 to 200 µm

Table 1. Compositions (wt%) of silicate phases in chondrule D8n.

	Interior region of chondrule D8n							Exterior region of chondrule D8n		
	Olivine phenocryst cores	Olivine overgrowths	Olivine near metal trails	Low-Ca pyroxene	Ca pyroxene	Mesostasis	Mixture[a]	Olivine	Ca pyroxene	Olivine in secondary chondrule
No. of grains	9	11	3	5	4	6		4	1	11
SiO_2	40.7	41.7	41.9	57.8	51.0	53.6	53.7	42.8	50.7	42.2
TiO_2	0.04	0.04	<0.04	0.34	1.2	0.40	0.0	<0.04	1.0	0.05
Al_2O_3	0.10	0.06	0.10	1.7	7.5	21.7	21.3	0.05	9.2	0.07
Cr_2O_3	0.61	0.50	0.63	0.70	0.81	0.44	0.0	0.41	1.1	0.25
FeO	7.5	1.6	3.8	1.1	0.50	0.42	0.0	1.0	0.97	0.71
MnO	0.20	0.14	0.20	0.10	0.11	0.10	0.0	0.10	0.42	0.09
MgO	51.0	55.6	54.1	36.6	19.8	8.2	7.9	56.7	20.1	56.7
CaO	0.21	0.22	0.20	1.5	19.0	15.1	17.1	0.18	17.8	0.35
Na_2O	<0.04	<0.04	<0.04	0.04	0.04	0.41	0.0	<0.04	<0.04	<0.04
K_2O	<0.04	<0.04	<0.04	<0.04	<0.04	0.05	0.0	<0.04	<0.04	<0.04
Total	100.4	99.9	100.9	99.9	100.0	100.4	100.0	101.2	101.3	100.4
Fa (mol%)	7.7	1.6	3.7					1.0		0.7
Fs (mol%)				1.6	0.8				1.6	
Wo (mol%)				2.9	40.5				38.3	

[a]Hypothetical mixture of pure endmember phases: 58 wt% anorthite, 21 wt% diopside, 11 wt% silica, and 10 wt% enstatite.

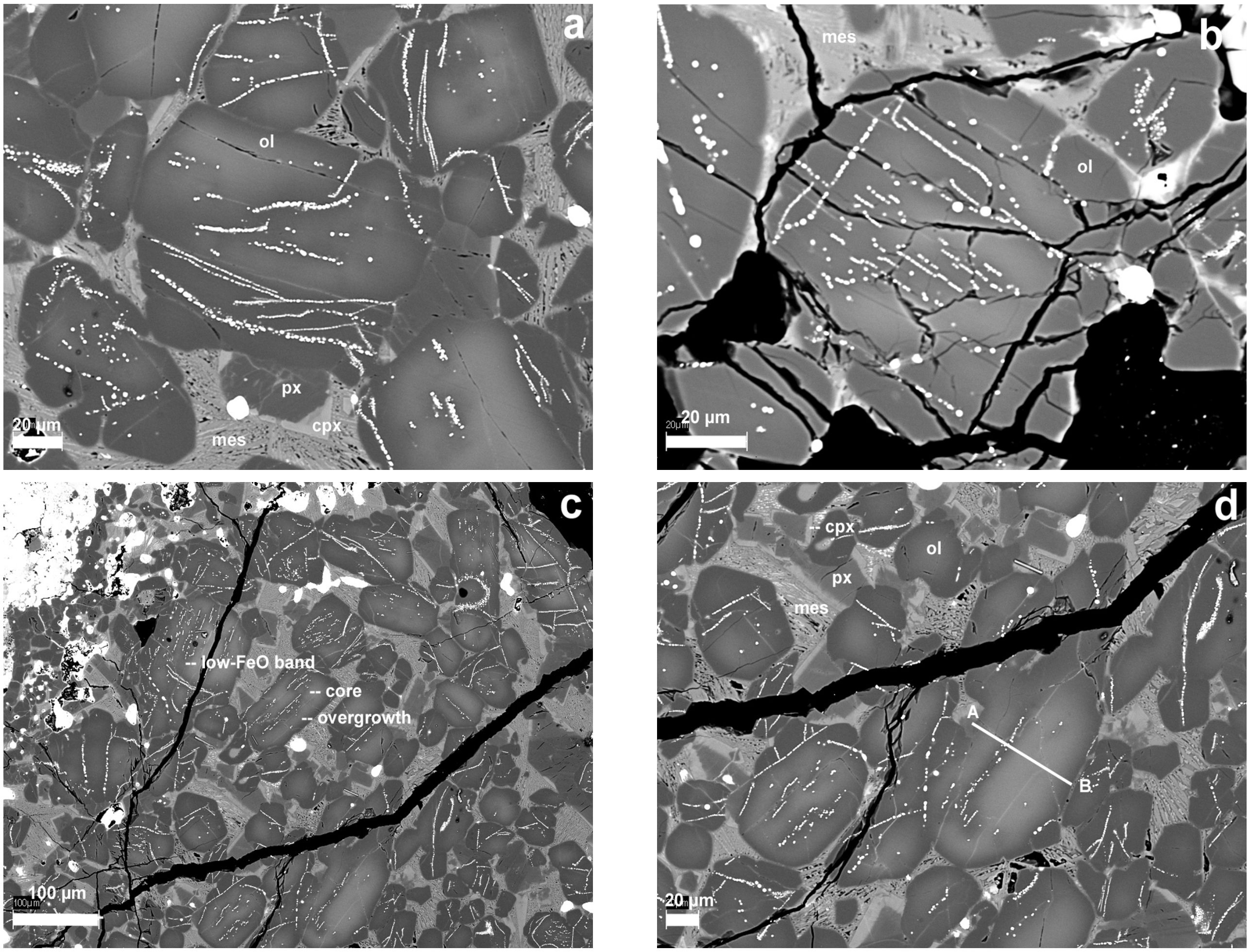

Fig. 2. BSE images of the interior region of the chondrule. a) Olivine phenocrysts (ol) with numerous curvilinear trails containing small blebs of low-Ni metallic Fe. As shown in the central phenocryst and the one at bottom right, many of the trails are subparallel to fractures. Below the central phenocryst is a small grain of low-Ca pyroxene (px, dark gray) with a rim of Ca pyroxene (cpx, light gray). Also present is vesicular mesostasis (mes). b) A high-magnification image of an olivine phenocryst (ol) containing numerous fractures and trails of metallic Fe blebs. Most of the trails are subparallel to each other and to the fracture trending NNW-SSE across the top of the phenocryst. A few trails on the left side of the phenocryst are perpendicular to the other trails and subparallel to a large fracture at the right side of the phenocryst. c) The moderately FeO-rich phenocryst cores (light gray) are surrounded by narrow low-FeO overgrowths (dark gray). Also visible in several phenocrysts are dark gray (low-FeO) bands flanking the curvilinear trails of metallic Fe blebs. A metal trail with an unusually large curvature occurs at upper right. d) A compositional zoning profile made across an olivine (ol) grain just to the right of center along line A-B is shown in Fig. 3. The mesostasis (mes, light gray) in chondrule D8n contains numerous elongated Ca pyroxene crystallites. Voids in between the crystallites are contraction cracks whose shapes are formed by the adjacent grains of Ca pyroxene. Low-Ca pyroxene grains (px, moderately light gray) with Ca pyroxene rims (cpx, light gray) are visible at top left and center.

and average ~60 µm. Every olivine grain in the interior is transected by several curvilinear trails (Figs. 2a and 2b) consisting of numerous aligned blebs (1–2 µm in diameter) of metallic Fe with no detectable Ni (Table 2). Many of the trails are subparallel, others intersect each other, and a few exhibit large curvatures (Fig. 2c). Many phenocrysts also contain some fractures, ~0.3 µm in width, with few or no metallic Fe blebs; most of these fractures are subparallel to some of the curvilinear trails of metal blebs (Figs. 2a and 2b). In some cases, the metal blebs appear to be aligned along olivine crystallographic directions (Fig. 2b).

A narrow (2–8 µm thick) band of relatively low-FeO (Fa_{3-5}) olivine flanks individual trails of metallic Fe grains within the olivine phenocrysts (Fig. 2c). Outside these bands, the cores of typical olivine phenocrysts have compositions of Fa_{7-10} and appear relatively bright in the BSE images (Figs. 2c and 2d).

Each olivine phenocryst is rimmed by an overgrowth 3–5 µm in thickness of low-FeO olivine (Fa_{1-2}) (Fig. 2c). These compositional variations are illustrated in the zoning profile across a representative olivine phenocryst (Fig. 3). The phenocryst cores are essentially unzoned; the dip in Fa in the diagram is due to the presence of the low-FeO olivine overgrowths.

Low-Ca pyroxene phenocrysts ($Fs_{0.7–2.5}Wo_{1.2–5.2}$) are euhedral and range in size from 5 to 40 µm. Each of these phenocrysts is surrounded by a rim of Ca-rich pyroxene ($Fs_{0.6–0.8}Wo_{39–42}$), 1.2–3.7 µm in thickness.

The mesostasis of the chondrule is mainly microcrystalline (crystallites that are 1–2 µm in thickness and 8–25 µm in length) with ~2–3 vol% glass and ~2–3 vol% voids; each void is 0.3–1.3 µm in size (Fig. 2d). The voids tend to have elongated shapes determined by the boundaries of adjacent Ca pyroxene crystallites (Fig. 2d); this indicates that the voids are not artifacts introduced during sample preparation. Also occurring in the mesostasis (Figs. 2a and 2c) are a few spheroidal and ellipsoidal blebs of Ni-poor kamacite (averaging 0.19 wt% Ni, <0.04 wt% Co) (Table 2), 9–20 µm in diameter. A few opaque blebs are composed of troilite. Most of the individual silicate grains in the mesostasis are too small to be analyzed quantitatively. The bulk composition of the mesostasis is rich in SiO_2, Al_2O_3, CaO, and MgO (Table 1) and corresponds fairly closely to a hypothetical mixture of 58 wt% anorthite, 21 wt% diopside, 11 wt% silica, and 10 wt% enstatite.

Exterior Region

The interior of chondrule D8n is surrounded by an exterior region (Figs. 1 and 4a), 45–140 µm in width, containing low-FeO olivine ($Fa_{0.9–1.5}$), low-FeO low-Ca pyroxene ($Fs_{0.7–0.8}Wo_{0.7–4.0}$), minor Ca-rich pyroxene ($Fs_{1.6}Wo_{38}$), feldspathic mesostasis, and abundant elongated and irregular grains of kamacite, troilite, pentlandite, and magnetite. None of the olivine grains in the exterior region contains trails of small metal blebs characteristic of dusty relicts. The high concentration of metal grains in the exterior region (Figs. 1 and 4a) mark the approximate boundary with the chondrule interior.

An opaque lump 960 µm in length and 260–540 µm in thickness occurs at the margin of chondrule D8n (Fig. 4b). The lump contains 30–50 µm-sized grains of troilite (concentrated toward the center) surrounded by kamacite; the troilite-kamacite assemblage is enclosed by a 70 µm thick rim of magnetite. Individual magnetite grains in this rim range from 5–75 µm in size.

An important question is whether this opaque lump is part of the chondrule or is instead an independent component of the meteorite matrix adjacent to the chondrule. It is difficult to be definitive, but the occurrence of large metal grains within and at the margins of many porphyritic chondrules in CR chondrites (Lee et al. 1992; Weisberg et al. 1993) suggests that large opaque nodules at chondrule margins may be genetically related to the adjacent chondrules. Furthermore, the presence of opaque clumps within shallow depressions at the surfaces of many ordinary-chondrite chondrules (i.e., "chondrule craters") (Gooding and Keil 1981) indicates that spinning partially molten chondrules can lose immiscible opaque clumps through centrifugal action (Grossman and Wasson 1985). By analogy, it seems likely that the opaque lump at the margin of chondrule D8n is an integral part of the chondrule. This conclusion is supported by the high abundance of metallic Fe-Ni in the adjacent exterior region of the chondrule.

Table 2. Compositions (wt%) of kamacite occurrences in chondrule D8n.

	Blebs in mesostasis	Trails in phenocrysts
No. of grains	3	1
Fe	100.6	100.2
Co	<0.04	<0.04
Ni	0.19	<0.04
Total	100.8	100.2

Secondary Chondrule

At one end of chondrule D8n, the exterior region contains a round object 170 µm in diameter that appears to be a secondary chondrule (Figs. 1 and 4c) consisting of olivine grains 15–35 µm in size; minor, low-Ca pyroxene grains 13 µm in size (with Ca pyroxene rims, 1–2 µm in thickness); blebs of kamacite 9 µm in diameter (containing 2.7–5.7 wt% Ni); and vesicular mesostasis. Olivine phenocrysts in the secondary chondrule are normally zoned with characteristic compositions ranging from $Fa_{0.6–0.8}$ in grain cores to $Fa_{0.7–1.0}$ in rims. The relatively high CaO content of the olivine in the secondary chondrule (0.35 wt%) (Table 1) reflects a moderately high CaO content in the precursor melt droplet (Libourel 1999).

One olivine phenocryst near the center of the secondary chondrule contains curvilinear trails of metallic Fe-Ni blebs (Fig. 4c), but does not seem to be FeO rich. The metal-bleb-bearing grain is similar in composition to the other grains in the secondary chondrule and shows slight normal zoning: it ranges from 0.67 wt% FeO ($Fa_{0.66}$) in the center to 0.72 wt% FeO ($Fa_{0.71}$) at the edge. It is possible, but far from certain, that the metal-bleb-bearing grain is relict.

Variations in Olivine Composition

Sizable variations in olivine composition are observed in chondrule D8n. Olivine in the secondary chondrule has the lowest concentrations of Cr_2O_3 (0.25 ± 0.08 wt%; 0.16–0.38 wt%), FeO (0.71 ± 0.10 wt%; 0.58–0.92 wt%) and MnO (0.09 ± 0.07 wt%; <0.04–0.24 wt%) in the entire chondrule. Olivine in the exterior region of the chondrule has higher concentrations of Cr_2O_3 (0.41 ± 0.01 wt%; 0.40–0.43 wt%) and FeO (1.0 ± 0.09 wt%; 0.88–1.1 wt%), but similar concentrations of MnO (0.10 ± 0.01 wt%; 0.09–0.11 wt%). The low-FeO overgrowths on the olivine phenocrysts in the interior region of the chondrule have even higher Cr_2O_3 (0.50 ± 0.10 wt%; 0.37–0.71 wt%), FeO (1.6 ± 0.84 wt%; 0.88–3.6 wt%), and MnO (0.14 ± 0.06 wt%; 0.08–0.31 wt%). The highest concentrations of these oxides occur in the interior region within olivine phenocryst cores (which all

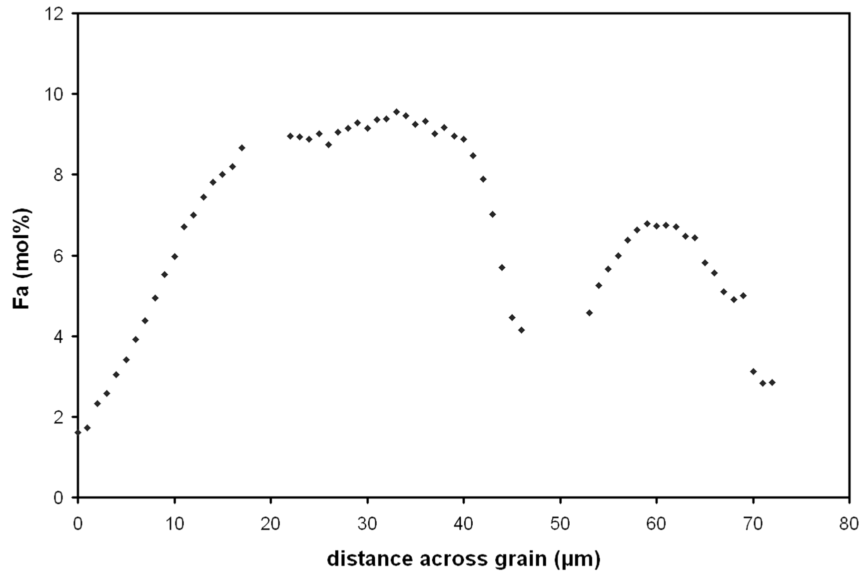

Fig. 3. A compositional zoning profile across line A-B of a typical olivine phenocryst in the interior region of chondrule D8n (cf. Fig. 2d). The overgrowths at the chondrule margin have much lower Fa contents than the phenocryst core. Point A is at the left side of the zoning profile at 0 µm; point B is at the right side of the zoning profile at ~72 µm. At a distance of ~50 µm from the left side, there is a low-FeO zone flanking a curvilinear trail of metallic Fe blebs. The missing Fa values at ~18 and 50 µm are points where the electron beam overlapped metal grains or fractures.

appear to be relict grains): the regions in these olivine grains away from the curvilinear trails of metal blebs have concentrations of Cr_2O_3 (0.61 ± 0.09 wt%; 0.50–0.74 wt%) and MnO (0.20 ± 0.02 wt%; 0.18–0.25 wt%) that are very similar to those of the olivine near the trails: Cr_2O_3 (0.63 ± 0.04 wt%; 0.59–0.68 wt%), and MnO (0.20 ± 0.03 wt%; 0.16–0.23 wt%). However, the FeO content in the olivine phenocrysts away from the trails (7.5 ± 1.0 wt%; 6.6–9.8 wt%) is considerably higher than that near the trails (3.8 ± 1.0 wt%; 2.8–4.7 wt%).

DISCUSSION

Origin of Chondrule D8n

History of Major Components

Because the cores of the olivine phenocrysts in the interior region of chondrule D8n are moderately FeO-rich (~7–10 wt% FeO), I conclude that D8n started off as a moderately FeO-rich, type II porphyritic olivine chondrule (Type II chondrules typically have olivine Fa contents between ~8 and 40 mole%.). The occurrence of numerous fractures within the olivine phenocrysts that are subparallel to many of the curvilinear arrays of metal blebs (Figs. 2a and 2b) indicates that these fractures are not artifacts produced during thin-section preparation or fragmentation on the parent asteroid.

The low-FeO olivine and abundant kamacite and troilite in the exterior region of the chondrule (Fig. 4a) and the large opaque lump at the chondrule margin (Fig. 4b) imply that the precursor of the interior region of D8n was transported from its formation location to a place where it became enmeshed in foreign material that consisted mainly of forsteritic olivine (with low FeO, MnO, and Cr_2O_3), metallic Fe-Ni, and sulfide (It is possible that some carbonaceous matter was also present, but direct petrographic evidence of this material is lacking. Nevertheless, graphite has been reported within clasts in another LL3 chondrite, i.e., Krymka; Semenenko and Girich 1995).

The forsterite- and metal-rich foreign material may have been a highly porous dust ball containing debris derived in large part from a disrupted low-FeO porphyritic chondrule. The low MnO of the forsterite in the foreign material may indicate that the forsterite precursor dust grains condensed from nebular gas prior to significant oxidation of Fe or appreciable condensation of Mn. (Manganese has a relatively low 50% condensation temperature: 1190 K at 10^{-4} atm and 1078 K at 10^{-6} atm) (Wasson 1985). The low Cr_2O_3 of the forsterite in the foreign material may reflect prior condensation of some Cr into metallic Fe-Ni (The olivine in this foreign material is not as primitive as the “refractory forsterites” described by Weinbruch et al. 2000; these latter grains contain lower FeO, MnO, and Cr_2O_3 and higher Al_2O_3 and TiO_2.).

Other possibilities suggested by reviewers for the genesis of the exterior region of D8n include 1) accretion to the primary chondrule of a crystal-laden melt, 2) formation by reduction via an external source of the outer portion of the

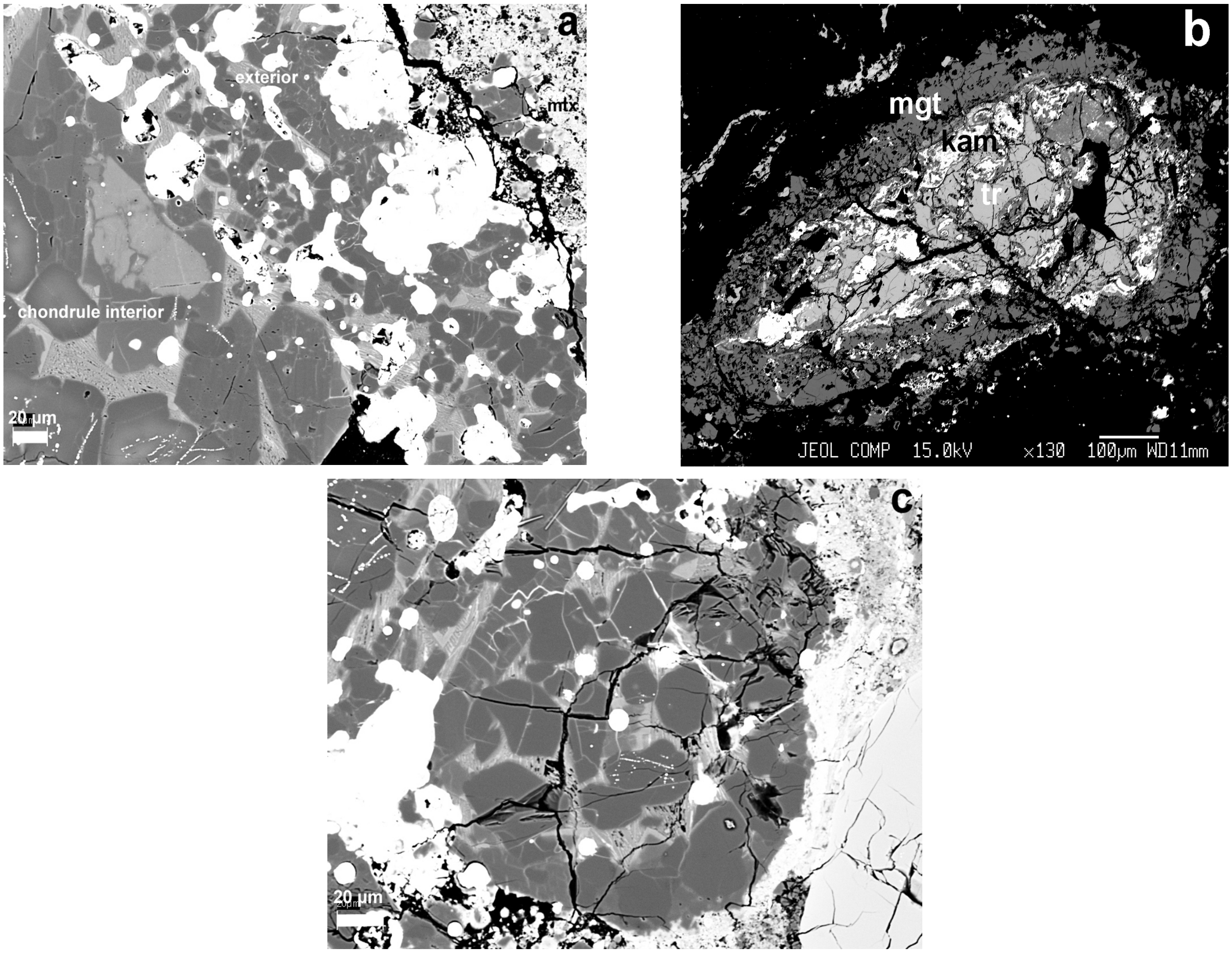

Fig. 4. BSE images of the exterior region of the chondrule. a) A swath of the exterior region running NW-SE. This region consists of large clusters of metal and troilite (white), small forsterite grains (dark gray), and mesostasis (light gray). The fine-grained matrix (mtx) of Semarkona is at the upper right; the interior region of the chondrule is at the bottom left. b) An opaque lump at one end of the exterior region of the chondrule. The lump consists mainly of kamacite (kam, white) and troilite (tr, light gray) surrounded by a thick rim of magnetite (mgt, dark gray). c) A small secondary chondrule at one end of the exterior region of the chondrule. It contains small forsterite grains, only one of which (center) contains curvilinear trails of metallic Fe blebs.

primary chondrule, and 3) formation by melting or partial melting of the primary chondrule. Because an isolated melt droplet would cool quickly (presumably within a few minutes), the first model would require that chondrule D8n was in close proximity to an object that was melted. In this case, the exterior region would be an adhering independent compound chondrule (cf. Wasson et al. 1995); many of these objects formed when a molten or partly molten object collided with a primary chondrule. This model cannot be ruled out. The second and third models are unlikely because there is a fairly sharp boundary between the interior region with its more ferroan olivines and the exterior region with highly reduced olivines. Reduction via an external source would probably result in more gradational olivine compositions.

On the other hand, there are numerous analogous examples of chondrules becoming enmeshed in fine-grained dust in the nebula. Such examples include:

1. Normal-size chondrules surrounded by microchondrule-bearing, fine-grained ferroan rims (Krot et al. 1997a). The rims served as a trapping matrix for molten droplets escaping the chondrule surface.
2. Coarse-grained igneous rims in CV and OC chondrites (Rubin 1984; Rubin and Wasson 1987; Krot and Wasson 1995). The rims formed by moderate-degree melting of fine-grained matrix-like rinds that surrounded the interior chondrules.
3. Independent enveloping compound chondrules (Wasson et al. 1995). Each secondary chondrule forms a quasi-spherical shell around the primary chondrule. The secondaries probably formed after their primary chondrule was coated with fine-grained materials. The conjoined object was heated in the nebula, but only the fine-grained outer region experienced significant melting.

The small secondary chondrule in the D8n assemblage probably started off as an independent type I PO chondrule. It is plausible that it collided with and became enmeshed within the foreign material destined to become the exterior region of D8n.

Melting of Conjoined Chondrule

The conjoined D8n object, which consisted of a moderately FeO-rich, type II PO chondrule surrounded by material rich in metal-sulfide and forsterite (and an embedded low-FeO chondrule), was partly melted in the nebula (in consonance with most modern models of chondrule formation, e.g., Hewins et al. 1996). I assume that it was a single event that melted the exterior region of the conjoined object and partly melted (and reduced) the original high-FeO primary chondrule. This is consistent with the apparent continuity of patches of mesostasis within the interior and exterior regions of D8n near the boundary between these zones. The abundance of metal and sulfide near this boundary suggests that the exterior region was metal-rich, that it was more extensively melted than the interior region, and that the metal-sulfide-rich melt wetted the surface of the primary object. Metal and sulfide mark the approximate boundary.

The secondary chondrule (Fig. 4c) contains ~75 wt% forsterite, ~20 wt% diopside, and ~5 wt% anorthitic mesostasis; isotherms from the equilibrium phase diagram for forsterite-diopside-anorthite (Osborn and Tait 1952) indicate that this bulk composition has a liquidus temperature of ~1750 °C. It is not clear if the secondary chondrule was appreciably melted during the event that caused the exterior region of the primary chondrule to melt.

The exterior region of chondrule D8n, which consists primarily of small olivine grains (with no dusty relicts) and rounded metal and sulfide blebs, underwent significant melting. However, the absence of skeletal olivine grains (indicative of rapid cooling) raises the possibility that melting was far from complete; in that case, many of the small olivine grains in the exterior region could be relict.

The liquidus temperature for the chondrule interior can be estimated from the forsterite-diopside-anorthite and forsterite-anorthite-silica equilibrium diagrams using the silicate-normalized, density-adjusted modal abundances of the interior's constituents (58 wt% olivine, 11 wt% low-Ca pyroxene, 2 wt% diopside, 29 wt% mesostasis) and the hypothetical end-member constituents of the mesostasis (58 wt% anorthite, 21 wt% diopside, 11 wt% silica, 10 wt% enstatite). Interpolation (and taking into account somewhat lower temperatures because of the moderate FeO content) yields a rough liquidus temperature of ~1600 °C (with an estimated uncertainty of approximately ±50 °C).

Phases with relatively low melting points (i.e., <1560 °C), including anorthitic mesostasis, low-Ca pyroxene, and Ca-rich pyroxene, were completely melted throughout the chondrule interior during this heating event. The outer portions of the moderately ferroan (Fa_{7-10}) olivine phenocrysts were partly resorbed, but the phenocryst interiors did not melt, presumably because too little heat was conducted in from the phenocryst surfaces during the period when the chondrule was near its peak temperature (If the interior grains had been appreciably smaller, they would have experienced more complete melting.). Because the phenocryst interiors melt at lower temperatures than that reached in the exterior region, and because olivine is subject to resorption, the final melting event must have been of short duration (see below).

The resorption of the outer portions of the moderately ferroan olivine phenocrysts in the interior region of D8n increased the concentrations of FeO, MnO, and Cr_2O_3 in the melt. As a result, the overgrowths on the phenocrysts crystallized from a melt that had higher concentrations of FeO, MnO, and Cr_2O_3 than did the olivines in the exterior region of D8n.

One reviewer suggested that the lower mean Cr_2O_3 content of the overgrowths relative to the cores is due in part to reduction of Cr^{2+} to Cr^0 and incorporation of the reduced Cr into metallic Fe (Rammensee et al. 1983; Zanda et al. 1994). The lower MnO contents of the overgrowths was ascribed to sequestration of MnO in the ferroan olivine cores. However, this seems unlikely because the olivine flanking the metal trails (which clearly formed by reduction) has about the same Cr_2O_3 and MnO contents as the phenocryst cores (Table 1). This indicates that reduction affected FeO, but not Cr_2O_3 or MnO. There is apparently no need to sequester MnO in the cores of the ferroan olivine grains.

Another reviewer suggested that the lower MnO and Cr_2O_3 contents of the olivine overgrowths relative to the cores may have resulted from evaporation of the melt and volatilization of Mn and Cr. This hypothesis may be consistent with the low concentrations of Na_2O (0.41 wt%) and K_2O (0.05 wt%) in the mesostasis relative to those of mean low-FeO (1.8 and 0.18 wt%) and high-FeO (4.1 and 0.58 wt%) porphyritic olivine chondrules in Semarkona (Jones and Scott 1989; Jones 1990). This possibility cannot be discounted.

G. E. Lofgren (personal communication, 2006) suggested that the interior of the chondrule may have been partly melted and reduced prior to acquiring the exterior region as a rim. Similar textures of olivine grains with metal blebs formed by reduction have been produced experimentally (Lofgren and Le 2002). In this model, the conjoined object would have been subsequently heated in an event that mainly melted the exterior region. The main argument against this scenario is the variation in olivine composition in the different regions of chondrule D8n as described above. The evidence seems most consistent with the model developed in the present manuscript.

Implications for External Heating and Rapid Chondrule Cooling

The petrographic evidence that the material at the chondrule margin was significantly melted and that the chondrule interior contains numerous unmelted relict olivine grains indicates that the heat source was external to the chondrule and that thermal equilibrium of the entire chondrule was not reached (A similar situation was described by Krot et al. [1997a], who observed normal-sized porphyritic chondrules that contain partly melted pyroxene grains at their margins. Because only these pyroxene grains were partly melted, it is apparent that these chondrules also were heated externally and that the heating mechanism preferentially affected the exterior, as might be expected from immersion in a plasma.).

The melt that was located in the exterior region of chondrule D8n mixed incompletely with that generated in the chondrule interior. The evidence for melt mixing lies in the intermediate Cr_2O_3, FeO, and MnO concentrations in the overgrowth olivines (Table 1). If mixing had been more thorough, the overgrowths on the olivine phenocrysts would have the same composition as the olivine in the exterior region of the chondrule. This indicates that chondrule melting was brief and that the chondrule cooled fairly rapidly.

The time it would take to mix the melt (not grow the olivine crystals which are assumed to be relict grains) can be estimated from the diffusion equation $D = r^2/4t$, where D is the diffusion coefficient, r is the mean radius of the chondrule (0.08 cm), and t is the time required for the attainment of 95% of the net mass transfer needed for complete equilibrium (Hofmann 1980). For a basaltic melt at 1650 °C, extrapolation of the Arrhenius lines for Fe and Mn plotted in Fig. 3.4 of Dunn (1986) yield diffusion coefficients of 5.6×10^{-6} cm^2 s^{-1} and 7.6×10^{-6} cm^2 s^{-1}, respectively. Solving the diffusion equation for t yields ~210 s for Mn and ~290 s for Fe. These values must be considered approximate because the melt of basaltic composition used in the experiments has appreciably more FeO (~9 versus 0.4 wt%) and somewhat less CaO (~10 versus 15 wt%) and Al_2O_3 (~18 versus 22 wt%) than the mesostasis in chondrule D8n. Cooling from ~1650 °C (the estimated liquidus temperature of the chondrule interior region) to ~800 °C (an estimate of the glass transition temperature) (e.g., Gooding and Keil 1981) over a period of ~300 s yields a cooling rate of ~3 °C s^{-1} (~10^4 °C hr^{-1}) (This calculation presupposes a linear cooling rate. Actual chondrule cooling by radiation would probably be highly non linear as the amount of radiation emitted from the cooling chondrule would decrease as the fourth power of temperature in accord with the Stefan-Boltzmann law.). Experimentally determined cooling rates of synthetic chondrules are typically much slower, in the range of 10–1000 °C hr^{-1} (e.g., Hewins et al. 2005); however, some workers (e.g., Yurimoto and Wasson 2002) have proposed much higher chondrule cooling rates (i.e., 10^5–10^6 °C hr^{-1}).

These calculations demonstrate that the time that the chondrule spent at peak temperatures was limited, but they do not quantitatively constrain the chondrule cooling rate. Nevertheless, it can be concluded that D8n most likely underwent cooling and crystallization within several minutes. This time scale is in agreement with that inferred for the formation of dusty olivines in chondrules by the experiments by Leroux et al. (2003).

Reduction

During the melting event, it seems plausible that a reducing agent (perhaps CO gas produced from graphite) (G. E. Lofgren 2006, personal communication) penetrated fractures in the ferroan olivine phenocrysts and caused reduction. If the reducing agent was carbon or CO, the reaction may have been similar to those of Reactions 1 or 2:

$$Fe_2SiO_4 + C \rightarrow FeSiO_3 + Fe + CO \tag{1}$$

$$Fe_2SiO_4 + CO \rightarrow FeSiO_3 + Fe + CO_2 \tag{2}$$

If the reducing agent was molecular hydrogen, then Reaction 3 may have obtained:

$$Fe_2SiO_4 + H_2 \rightarrow FeSiO_3 + Fe + H_2O \tag{3}$$

The Fe_2SiO_4 (fayalite) component of the olivine phenocrysts was reduced in a narrow zone flanking the fractures (Fig. 2c); metallic Fe was produced and formed small spheroidal blebs at the sides of the fractures. The $FeSiO_3$ (ferrosilite) component may have been subjected to fluid transport through the fractures to nearby crystallizing pyroxene grains. The CO, CO_2, or H_2O gases produced during the reduction reaction probably escaped from the melt, consistent with the occurrence of 2–3 vol% voids in the mesostasis.

However, some olivine grains possess crystallographically oriented metal blebs, indicating that some of the reduction occurred within the crystal lattice. Leroux et al. (2003) conducted TEM studies of dusty olivines and concluded that subsolidus reduction of fayalite took place via Reaction 4:

$$Fe_2SiO_{4\ \text{in olivine}} = 2Fe_{\text{metal}} + xSiO_{2\ \text{in melt}} + (1-x)\ SiO_{\text{in gas}} + (3-x)/2O_{2\ \text{in gas}} \tag{4}$$

Although the stoichiometric relationships are unknown, the reaction indicates incomplete movement of the Si and O move from the inside to the outside of the olivine phenocrysts, causing a diminishment of Si in the dusty reduced zones (Leroux et al. 2003).

Irrespective of the reaction involved, the FeO contents of the olivine flanking the metal-bearing trails were reduced, but the concentrations of Cr_2O_3 and MnO remained unchanged. This behavior is expected because Cr and Mn are less noble (i.e., more likely to remain as oxides) than Fe.

Because chondrule D8n was only partly reduced, it is straightforward to determine the extent of reduction. Interior olivine regions distant from reduction zones have mean compositions of approximately Fa8. The reduced olivine grains flanking the fractures have mean compositions of approximately Fa4. The difference in Fa compositions (4 mole%) corresponds to the reduction of ~4 wt% FeO to ~3 wt% metallic Fe. This degree of reduction is similar to that inferred by Jones (1996) for other OC chondrules with dusty olivine grains.

Crystallization Sequence

Superposition textures indicate that the first phase to crystallize from the melt in the interior region of D8n was forsteritic olivine, which formed overgrowths on the relict ferroan olivine (Fig. 2c). Low-Ca pyroxene occurs at the margins of many olivine grains (e.g., Fig. 2a). The presence of Ca pyroxene rims on many low-Ca pyroxene grains (Fig. 2a) indicates that Ca pyroxene crystallized next. Immiscible metal and sulfide blebs formed droplets in the residual silicate-rich melt (Fig. 2c); their liquidus temperatures (~1535 °C for the low-Ni metallic Fe and 988 °C for the Fe-FeS eutectic) are below that estimated above for the chondrule interior liquidus temperature, i.e., ~1600 °C. The metal and sulfide blebs solidified when the mesostasis quenched.

Parent-Body Aqueous Alteration

As described above, the large opaque lump at the margin of chondrule D8n (Fig. 4c) has an interior consisting of troilite and kamacite surrounded by a rim of magnetite, 70 μm in thickness. This lump was probably initially composed completely of kamacite and troilite. Long after chondrule formation and agglomeration, parent-body aqueous alteration caused oxidation of the kamacite in the outer portion of this lump to form the magnetite rim. Opaque phases in the exterior region of chondrule D8n include kamacite, troilite, magnetite and pentlandite. Oxidation of kamacite liberated Ni; because little Ni entered magnetite, the Ni partitioned to some extent into the pentlandite.

Aqueous alteration in Semarkona has been documented previously by the occurrences of abundant phyllosilicate (i.e., Fe-rich smectite) in the matrix (Hutchison et al. 1987; Alexander et al. 1989) and of opaque assemblages outside chondrules that contain magnetite, carbide, kamacite, troilite, Ni-rich metal and pentlandite (Taylor et al. 1981; Krot et al. 1997b).

Compositional Evolution of Nebular Solids

The compositions of fine-grained materials in equilibrium with gas in the solar nebula changed with time as the nebula cooled. At ambient temperatures above ~750 K, little FeO (<1 mol% Fa) should occur in fine-grained olivine that could potentially serve as chondrule precursor materials (Grossman and Larimer 1974). Any chondrules that formed in the nebula at ambient temperatures above this value should contain very low FeO. At ambient nebular temperatures below 500 K, fine-grained olivine should contain ~15 mol% Fa (J. T. Wasson, personal communication, 2005). Chondrules that formed from materials in equilibrium with the gas at this ambient temperature should be relatively rich in FeO. The overall trend then would be that low-FeO chondrules formed before high-FeO chondrules; this trend is consistent with the occurrence of low-FeO relict grains in high-FeO chondrules. In fact, Wasson and Rubin (2003) found that >90% of high-FeO porphyritic chondrules in CO3.0 chondrites contain low-FeO relict grains.

The trend of increasing amounts of FeO in fine-grained nebular materials with time is consistent with the occurrence of ferroan coarse-grained, igneous rims on ~50% of CV3 chondrules (most of which are low-FeO porphyritic chondrules) (Rubin 1984) and the presence of ferroan fine-grained matrix-like rims with numerous microchondrules (including rare fayalitic microchondrules) around some normal-size low-FeO porphyritic and barred-olivine chondrules in OC (Krot et al. 1997a). Because all of these rims formed after the chondrules they surround, the trend is clear of increasing FeO in fine-grained nebular materials with time.

The trend is also consistent with the observation of Wasson et al. (1995) that, among independent compound chondrules, most secondaries (which formed later) have higher FeO/(FeO + MgO) ratios than primaries.

The $\Delta^{17}O$ values of nebular materials appear to increase with FeO content (Jones et al. 2000; Wasson et al. 2004; Kunihiro et al. 2004, 2005); low-FeO porphyritic chondrules and low-FeO relict grains inside high-FeO porphyritic chondrules tend to have low $\Delta^{17}O$ values.

Contrary to the expected trend of FeO increasing with time, there are numerous examples of high-FeO relict grains within low-FeO chondrules. This would include most instances of dusty ferroan olivine relicts in low-FeO porphyritic chondrules (e.g., Rambaldi 1981; Nagahara 1981; Rambaldi and Wasson 1982; Kracher et al. 1984; Jones 1996). It also includes Semarkona chondrule D8n, a high-FeO chondrule from the present study that became enmeshed in low-FeO material and was then remelted.

An important question is whether the common occurrence of ferroan relicts in magnesian chondrules indicates that, in general, low-FeO and high-FeO chondrules are essentially contemporaneous.

I think it more likely that the occurrence of high-FeO relicts within low-FeO chondrules reflects the stochastic nature of inelastic collisions of materials in the nebula and the frequency of chondrule melting events. After the nebula cooled below 500 K and the first generations of both low-FeO and high-FeO chondrules had formed, these objects and their fragments were in close proximity and suffered collisions. Some collisions were inelastic (presumably in those instances when one or both of the colliding objects was partly molten) and resulted in conjoined (occasionally compositionally disparate) objects. This is indicated by the common occurrence of low-FeO relict grains (presumed to be fragments of low-FeO porphyritic chondrules) in high-FeO porphyritic CO chondrules (Wasson and Rubin 2003).

The presence of fine-grained ferroan dust in which chondrules could become enmeshed is indicated by the presence of microchondrule-bearing ferroan matrix-like rims around some normal-sized OC chondrules (Krot et al. 1997a) as well as by ferroan igneous rims on ~50% of CV3 chondrules (Rubin 1984).

Random chondrule-formation-related heating events caused remelting of single chondrules, compound chondrules, and chondrules enmeshed in fine-grained materials. In many cases, the conjoined objects had appreciably different FeO/(FeO + MgO) contents.

Acknowledgments–I thank the curators at the American Museum of Natural History for the loan of Semarkona thin section AMNH 4128-2. I am grateful to J. T. Wasson for suggestions and to A. Pack, H. C. Connolly, H. Nagahara, R. H. Hewins, R. H. Jones, G. E. Lofgren, A. Ruzicka, and C. Floss for comments and suggestions on different versions of this manuscript. This work was supported in part by NASA grant NAG5-12967.

Editorial Handling—Dr. Christine Floss

REFERENCES

Alexander C. M. O.'D, Hutchison R., and Barber D. J. 1989. Origin of chondrule rims and interchondrule matrices in unequilibrated ordinary chondrites. *Earth and Planetary Science Letters* 95: 187–207.

Dunn T. 1986. Diffusion in silicate melts: An introduction and literature review. In *Silicate melts: Their properties and structure applied to problems in geochemistry, petrology, economic geology and planetary geology,* edited by Scarfe C. M. Ottawa: Mineralogical Association of Canada. pp. 57–92.

Gooding J. L. and Keil K. 1981. Relative abundances of chondrule primary textural types in ordinary chondrites and their bearing on conditions of chondrule formation. *Meteoritics* 16:17–43.

Grossman J. N. and Wasson J. T. 1985. The origin and history of the metal and sulfide components of chondrules. *Geochimica et Cosmochimica Acta* 49:925–939.

Grossman J. N., Rubin A. E., Nagahara H., and King E. 1988. Properties of chondrules. In *Meteorites and the early solar system,* edited by Kerridge J. F. and Mathews M. S. Tucson, Arizona: The University of Arizona Press. pp. 619–659.

Grossman L. and Larimer J. W. 1974. Early chemical history of the solar system. *Reviews of Geophysics and Space Physics* 12:71–101.

Hewins R. H. 1988. Experimental studies of chondrules. In *Meteorites and the early solar system,* edited by Kerridge J. F. and Matthews M. S. Tucson, Arizona: The University of Arizona Press. pp. 660–679.

Hewins R. H., Jones R. H., and Scott E. R. D, editors. 1996. *Chondrules and the protoplanetary disk.* New York: Cambridge University Press. 346 p.

Hewins R. H., Connolly H. C., Lofgren G. E., and Libourel G. 2005. Experimental constraints on chondrule formation. In *Chondrites and the protoplanetary disk,* edited by Krot A. N., Scott E. R. D., and Reipurth B. San Francisco: Astronomical Society of the Pacific. pp. 286–316.

Hofmann A. W. 1980. Diffusion in natural silicate melts: A critical review. In *Physics of magmatic processes,* edited by Hargraves R. B. Princeton, New Jersey: Princeton University Press. pp. 385–417.

Hutchison R., Alexander C. M. O'D., and Barber D. J. 1987. The Semarkona meteorite: First recorded occurrence of smectite in an ordinary chondrite and its implications. *Geochimica et Cosmochimica Acta* 51:1875–1882.

Jones R. H. 1990. Petrology and mineralogy of Type II, FeO-rich chondrules in Semarkona (LL3.0): Origin by closed-system fractional crystallization, with evidence of supercooling. *Geochimica et Cosmochimica Acta* 54:1785–1802.

Jones R. H. 1992. On the relationship between isolated and chondrule olivine grains in the carbonaceous chondrite ALHA77307. *Geochimica et Cosmochimica Acta* 56:467–482.

Jones R. H. 1996. Relict grains in chondrules: Evidence for chondrule recycling. In *Chondrules and the protoplanetary disk,* edited by Hewins R. H., Jones R. H., and Scott E. R. D. New York: Cambridge University Press. pp. 163–172.

Jones R. H. and Danielson L. R. 1995. A chondrule origin for dusty, relict olivine grains (abstract). 26th Lunar and Planetary Science Conference. pp. 699–700.

Jones R. H. and Scott E. R. D. 1989. Petrology and thermal history of type IA chondrules in the Semarkona (LL3.0) chondrite. Proceedings, 19th Lunar and Planetary Science Conference. pp. 523–536.

Jones R. H., Saxton J. M., Lyon I. C., and Turner G. 2000. Oxygen isotopes in chondrule olivine and isolated olivine grains from the CO3 chondrite Allan Hills A77307. *Meteoritics & Planetary Science* 35:849–857.

Kracher A., Scott E. R. D., and Keil K. 1984. Relict and other anomalous grains in chondrules: Implications for chondrule formation. Proceedings, 14th Lunar and Planetary Science Conference. pp. B559–B566.

Krot A. N. and Wasson J. T. 1995. Igneous rims on low-FeO and high-FeO chondrules in ordinary chondrites. *Geochimica et Cosmochimica Acta* 59:4951–4966.

Krot A. N., Rubin A. E., Keil K., and Wasson J. T. 1997a. Microchondrules in ordinary chondrites: Implications for chondrule formation. *Geochimica et Cosmochimica Acta* 61: 463–473.

Krot A. N., Zolensky M. E., Wasson J. T., Scott E. R. D., Keil K., and Ohsumi K. 1997b. Carbide-magnetite assemblages in type 3 ordinary chondrites. *Geochimica et Cosmochimica Acta* 61:219–237.

Kunihiro T., Rubin A. E., McKeegan K. D., and Wasson J. T. 2004. Oxygen-isotopic compositions of relict and host grains in chondrules in the Yamato-81020 CO3.0 chondrite. *Geochimica et Cosmochimica Acta* 68:3599–3606.

Kunihiro T., Rubin A. E., and Wasson J. T. 2005. Oxygen-isotopic compositions of low-FeO relicts in high-FeO host chondrules in Acfer 094, a type 3.0 carbonaceous chondrite closely related to CM. *Geochimica et Cosmochimica Acta* 69:3831–3840.

Lee M. S., Rubin A. E., and Wasson J. T. 1992. Origin of metallic Fe-Ni in Renazzo and related chondrites. *Geochimica et Cosmochimica Acta* 56:2521–2533.

Leroux H., Libourel G., Lemelle L., and Guyot F. 2003. Experimental study and TEM characterization of dusty olivines in chondrites: Evidence for formation by in situ reduction. *Meteoritics & Planetary Science* 38:81–94.

Libourel G. 1999. Systematics of calcium partitioning between olivine and silicate melt: Implications for melt structure and calcium content of magmatic olivines. *Contributions to Mineralogy and Petrology* 136:63–80.

Lofgren G. E. 1989. Dynamic crystallization of chondrule melts of porphyritic olivine composition: Textures experimental and natural. *Geochimica et Cosmochimica Acta* 53:461–470.

Lofgren G. E. and Le L. 2002. Experimental replication of relict "dusty" olivine in type 1B chondrules (abstract). *Meteoritics & Planetary Science* 37:A90.

Lofgren G. E. and Russell W. J. 1986. Dynamic crystallization of chondrule melts of porphyritic and radial pyroxene composition. *Geochimica et Cosmochimica Acta* 50:1715–1726.

Nagahara H. 1981. Evidence for secondary origin of chondrules. *Nature* 292:135–136.

Nagahara H. 1983. Chondrules formed through incomplete melting of the pre-existing mineral clusters and the origin of chondrules. In *Chondrules and their origins,* edited by King E. A. Houston, Texas: Lunar and Planetary Institute. pp. 211–222.

Osborn E. F. and Tait D. B. 1952. The system diopside-forsterite-anorthite. *American Journal of Science,* Bowen volume. pp. 413–433.

Rambaldi E. R. 1981. Relict grains in chondrules. *Nature* 293:558–561.

Rambaldi E. R. and Wasson J. T. 1982. Fine, nickel-poor Fe-Ni grains in the olivine of unequilibrated ordinary chondrites. *Geochimica et Cosmochimica Acta* 46:929–939.

Rammensee W., Palme H., and Wänke H. 1983. Experimental investigation of metal-silicate partitioning of some lithophile elements (Ta, Mn, V, Cr) (abstract). Proceedings, 14th Lunar and Planetary Science Conference. pp. 628–629.

Rubin A. E. 1984. Coarse-grained chondrule rims in type 3 chondrites. *Geochimica et Cosmochimica Acta* 48:1779–1789.

Rubin A. E. and Wasson J. T. 1987. Chondrules, matrix and coarse-grained chondrule rims in the Allende meteorite: Origin, interrelationships and possible precursor components. *Geochimica et Cosmochimica Acta* 51:1923–1937.

Semenenko V. P. and Girich A. L. 1995. Mineralogy of a unique graphite-containing fragment in the Krymka chondrite (LL3). *Mineralogical Magazine* 59:443–454.

Steele I. M. 1989. Compositions and textures of relic forsterite in carbonaceous and unequilibrated ordinary chondrites. *Geochimica et Cosmochimica Acta* 53:2069–2079.

Taylor G. J., Okada A., Scott E. R. D., Rubin A. E., Huss G. R., and Keil K. 1981. The occurrence and implications of carbide-magnetite assemblages in unequilibrated ordinary chondrites (abstract). Proceedings, 12th Lunar and Planetary Science Conference. pp. 1076–1078.

Wasson J. T. 1985. *Meteorites: Their record of early solar-system history.* New York: W. H. Freeman & Company.

Wasson J. T. and Rubin A. E. 2003. Ubiquitous relict grains in type II chondrules, narrow overgrowths, and chondrule cooling rates following the last melting event. *Geochimica et Cosmochimica Acta* 67:2239–2250.

Wasson J. T., Krot A. N., Lee M. S., and Rubin A. E. 1995. Compound chondrules. *Geochimica et Cosmochimica Acta* 59:1847–1869.

Wasson J. T., Rubin A. E., and Yurimoto H. 2004. Evidence in CO3.0 chondrules for a drift in the O isotopic composition of the solar nebula. *Meteoritics & Planetary Science* 39:1591–1598.

Weinbruch S., Palme H., and Spettel B. 2000. Refractory forsterite in primitive meteorites: Condensates from the solar nebula? *Meteoritics & Planetary Science* 35:161–171.

Weisberg M. K., Prinz M., Clayton R. N., and Mayeda T. K. 1993. The CR Renazzo-type carbonaceous chondrite group and its implications. *Geochimica et Cosmochimica Acta* 57:1567–1586.

Yu Y. and Hewins R. H. 1998. Transient heating and chondrule formation: Evidence from sodium loss in flash heating simulation experiments. *Geochimica et Cosmochimica Acta* 62:159–172.

Yurimoto H. and Wasson J. T. 2002. Extremely rapid cooling of a carbonaceous-chondrite chondrule containing ^{16}O-rich olivine and a ^{26}Mg-excess. *Geochimica et Cosmochimica Acta* 66:4355–4363.

Zanda B., Bourot-Denise M., Perron C., and Hewins R. H. 1994. Origin and metamorphic redistribution of silicon, chromium, and phosphorus in the metal of chondrites. *Science* 265:1846–1849.